Article

A Multifunctional and Fast-Response Lysosome-Targetable Fluorescent Probe for Monitoring pH and Isoxaflutole

Liu Yang, Yan Liu, Mingli Yue, Ping Li, Yulong Liu [ID]**, Fei Ye *** [ID] **and Ying Fu *** [ID]

Department of Applied Chemistry, College of Arts and Sciences, Northeast Agricultural University, Harbin 150030, China; yangliu@neau.edu.cn (L.Y.); liuyansjm@163.com (Y.L.); yuemingli@neau.edu.cn (M.Y.); liping@neau.edu.cn (P.L.); liuyulong@neau.edu.cn (Y.L.)
* Correspondence: yefei@neau.edu.cn (F.Y.); fuying@neau.edu.cn (Y.F.)

Abstract: A new chemosensor, namely *N*-(2-morpholinoethyl)acetamide-4-morpholine-1,8-naphthimide (**MMN**), was designed and synthesized through an amidation reaction. **MMN** was fabricated as a multifunctional fluorescent probe for monitoring pH and isoxaflutole. **MMN** exhibited excellent stability in MeCN/H$_2$O (*v/v*, 9/1), with an obvious "off–on" fluorescence response toward pH changes due to intramolecular charge transfer (ICT), where the linear response ranges of **MMN** in the weakly acidic system were from 4.2 to 5.0 and from 5.0 to 6.0 with apparent pK_a = 4.62 ± 0.02 and 5.43 ± 0.02. Based on morpholine as the lysosome targetable unit, **MMN** could selectively locate lysosomes in live cells. **MMN** also successfully detected the presence of H$^+$ in test papers. Finally, **MMN** could specifically recognize isoxaflutole at a detection limit of 0.88 μM. A possible sensing mechanism was identified based on density function theory calculations. These results indicate that **MMN** could be a superior potential chemosensor for detecting pH and isoxaflutole selectively and sensitively and could be used in real sample detection.

Keywords: fluorescence; pH sensing; lysosome target probe; isoxaflutole; ICT

1. Introduction

pH is essential to human life and plays vital roles in some physiological and chemical processes, including enzymatic activity, cell function, environmental monitoring and human tissue fluid [1]. Intracellular pH homeostasis is necessary for the regulation of various basic cellular processes to maintain normal cell function [2–4]. Lysosomes, as essential acidic subcellular organelles (pH 4.5–5.5) in eukaryotic cells, participate in intracellular digestion and cellular differentiation [5,6]. Monitoring lysosome pH change is very important in the development of medical diagnoses and treatment methods. Hence, exploring a more effective strategy for the accurate detection of pH is crucial.

In the past few years, various techniques have been used for pH detection such as the colorimetric method [7], electrochemistry procedures [8], ion-sensitive field-effect transistors [9] and fluorescence techniques [10]. However, there are still shortcomings such as photobleaching, high background emission, alkalization, complicated sample preparation, the need for sophisticated instruments, and high time-consumption and costs. Despite these limitations, fluorescent techniques have the advantages of being convenient, efficient, sensitive and selective and have the potential to be used for monitoring pH.

Pesticides refer to chemical agents used in agriculture to control pests and to regulate plant growth. Pesticides are widely used in agriculture, forestry and animal husbandry; in environmental and family hygiene, pest control and epidemic prevention; and in industrial products to prevent mildew and moths [11]. Isoxaflutole is a highly effective preseedling herbicide that is used in maize, sugarcane and other dry crop fields [12–14]. However, the long-term application of pesticides across wide areas not only bring potential health risks to humans but also cause environmental pollution [15–17]. The negative impact of pesticide residue has thus aroused people's attention.

Current reports on the detection methods for isoxaflutole residue mainly involve liquid chromatography and liquid chromatography-tandem mass spectrometry [18,19]. Even though the chromatography method has the advantages of being highly sensitive, having a superior separation ability and having excellent selectivity, this method has a long pretreatment time and can have interferences in the detection process. It can also be costly and requires the presence of highly selective detectors for detecting pesticides. A more accurate, fast, efficient and convenient method in the detection of pesticides is needed. Chemosensors such as fluorescent probes have the potential to detect isoxaflutole with the advantages of low costs, easy operation, fast signal response and signal visualization.

A new lysosome-targetable pH fluorescent probe, namely *N*-(2-morpholinoethyl)acetamide-4-morpholine-1,8-naphthimide (**MMN**), was synthesized and characterized. **MMN** was synthesized by introducing the morpholine unit [20–22] as a lysosomal targeting group to naphthalimide, which was highly sensitive to pH changes due to intramolecular charge transfer (ICT) [23]. The fluorescence intensity of **MMN** increased linearly to 2.2 times in the apparent pH range from 4.2 to 6.0, and the apparent pK_a was 4.62 ± 0.02 and 5.43 ± 0.02. The proposed sensing mechanism was confirmed by ^{1}H NMR. **MMN** selectively located lysosomes in live cells and successfully detected H$^+$ in test papers. Additionally, **MMN** could specifically recognize isoxaflutole at a detection limit of 0.88 μM.

## 2. Results and Discussion

2.1. Design and Synthesis of *MMN*

Naphthalimide, as a representative of fluorophore, shows a high fluorescence quantum yield and high thermal stability [24,25]. Morpholine has been recognized for its special lysosomal targeting function [26]. Based on a rational design, **MMN** was synthesized through an amidation reaction, as illustrated in Scheme 1. The fluorescent probe was characterized by FTIR, ^{1}H NMR, ^{13}C NMR and HRMS spectroscopy. **MMN** exhibited an obvious "off–on" fluorescence response toward pH changes and detected isoxaflutole.
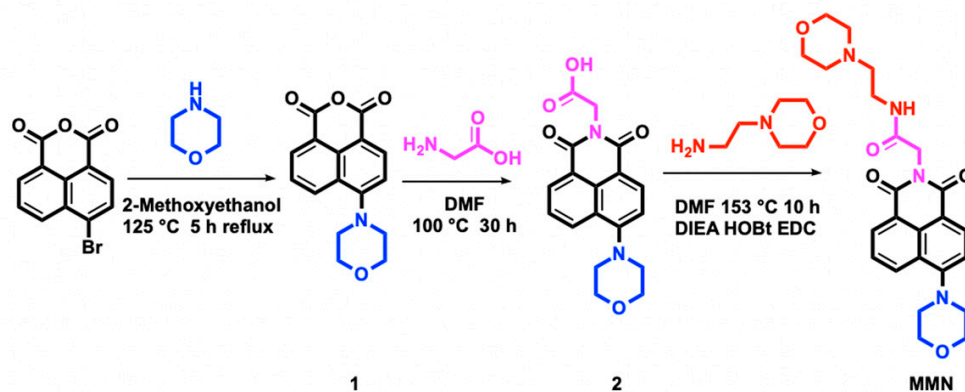
Scheme 1. Synthetic route of **MMN**.

2.2. pH-Dependent Sensing Performance

The solvent effect of **MMN** was studied through fluorescence measurements in different solvents (Figure S1). Based on the solvent fluorescence response and a low toxicity, the spectral properties of **MMN** were investigated in CH$_3$CN/H$_2$O (*v/v*, 9/1) where the apparent pH was 6.0. The fluorescence spectra of **MMN** exhibited a striking dependence on pH (Figure 1a). **MMN** showed a weak fluorescence signal at 529 nm in the strongly acidic apparent pH region (pH < 4.2). When the alkalinity of the solution increase to weakly alkaline (pH > 6.0), the fluorescence intensity increased significantly, with a slow blueshift by 6 nm.
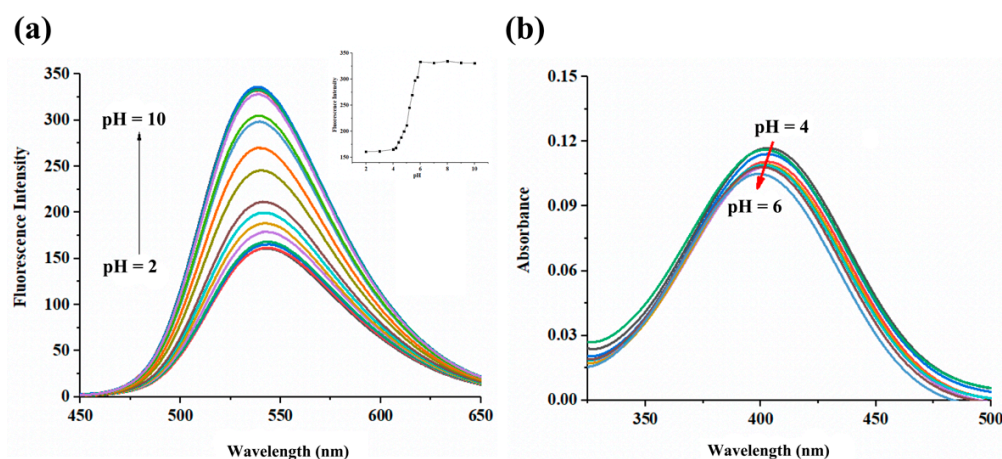
Figure 1. Effect of pH on (**a**) fluorescence and (**b**) UV–Vis absorption spectra of **MMN** at concentrations of 1.00×10^{-5} M. Inset: The maximum fluorescence intensity of **MMN** in different pH solutions at 529 nm.

To further evaluate the dependence of **MMN** on pH, the UV–Vis spectra of **MMN** at different pH values were investigated. As the pH values of the solution increased, a blueshift of the UV absorption band was observed (Figure 1b). **MMN** displayed a superior "off–on" switching behavior from apparent pH 2 to 10 and demonstrated an obvious change in the electron density of naphthalene rings, which was consistent with the fluorescent emission spectra analyses. The fluorescence spectra of **MMN** were investigated to examine its anti-interference in the presence of other ions at a representative pH value (pH = 4.2). As shown in Figure S2, **MMN** possesses the potential to accurately detect pH changes with negligible interference.

2.3. pK_a Value, Reversibility and Photostability

As shown in Figure 2a, the fluorescence intensity of **MMN** expressed an excellent partitioned response to pH, i.e., the partitioned linear ranges of apparent pH were from 4.2 to 5.0 with a correlation coefficient (R^2) of 0.99 and from 5.0 to 6.0 with an R^2 of 0.99. The fluorescence intensity of **MMN** with different apparent pH values was used to calculate the acidity-constant apparent pK_a values of **MMN** based on the Henderson–Hasselbalch equation in MeCN/H$_2$O (v/v, 9/1):

$$pK_a = pH - log\left(\frac{I_{max} - I}{I - I_{min}}\right)$$

where I is the observed fluorescence intensity at a fixed wavelength, and I_{max} and I_{min} are the corresponding maximum and minimum intensities, respectively [27]. These results indicated that **MMN** exhibited a high sensitivity to weakly acidic pH with apparent pK_a values of 4.62 ± 0.02 and 5.43 ± 0.02. The reversibility behavior of the prepared **MMN** probe was investigated by tracking the changes in emission intensity at 529 nm at apparent pH 4.2 and pH 6.0 (Figure 2b). The changes in colors (inset of Figure 2b) were recorded at apparent pH 4.2 and 6. There was no significant change in the reversibility up to four cycles. Thus, this proved that **MMN** could be used as a reversible pH monitor due to its excellent reversibility. In Figure 2c, the response of the proposed **MMN** to H$^+$ was in real time, and the fluorescence intensity remained nearly unchanged over 130 min when tested at apparent pH 4.2 and 6.0. The results indicated that **MMN** could be reliably applied for real-time monitoring of pH in practical applications.
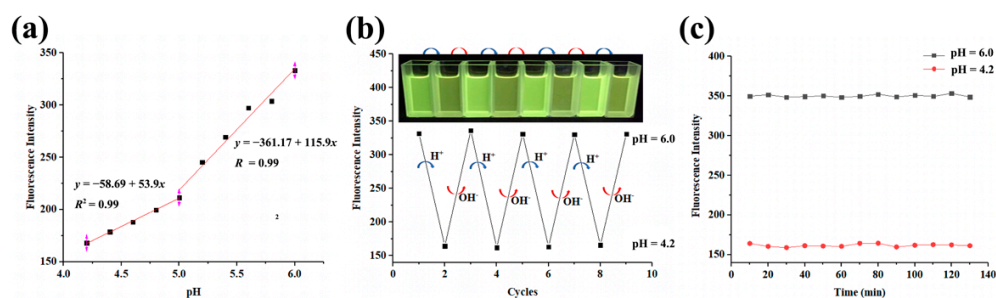
Figure 2. (**a**) The linear responses of fluorescence intensity. (**b**) Reversibility of the fluorescence intensity of **MMN** between apparent pH 4.2 and 6.0. Inset: The color changes of **MMN** solution under UV light of 365 nm. (**c**) Changes in the fluorescence intensities of **MMN** with times among nonacidic and acid conditions.

2.4. Recognition Mechanism of MMN to H⁺

To examine the proposed interactive mechanism of **MMN** on the pH value, ^{1}H NMR spectra of **MMN** (D$_2$O/DMSO-d_6 (*v*/*v*, 1:1)) were measured by adding TFA (H$^+$) or NaOH (OH$^-$) to solutions. As shown in Figure 3a, upon the addition of H$^+$ to **MMN**, the signal at δ 8.10–8.13 ppm was downfield-shifted to 8.45–8.47 ppm owing to a decrease in the electron density around N-H of amide induced by H$^+$. The signal of the aromatic protons (Ar-H) was not affected except for a later peak fraction. However, the ^{1}H NMR spectrum of **MMN + OH$^-$** was consistent with that of **MMN**. Therefore, when H$^+$ was added, the change in ^{1}H NMR spectrum contributed to a decrease in electron density around N-H of amide and the active hydrogen protons NH produced a charge transfer process, where N atom was positively charged and C=N was formed due to tautomerism. When OH$^-$ was added, the intramolecular charge transfer (ICT) effect was weakened, and a blueshift and enhancement of the fluorescent emission band were observed [23]. The mechanism of **MMN** for H$^+$ is proposed in Figure 3b.
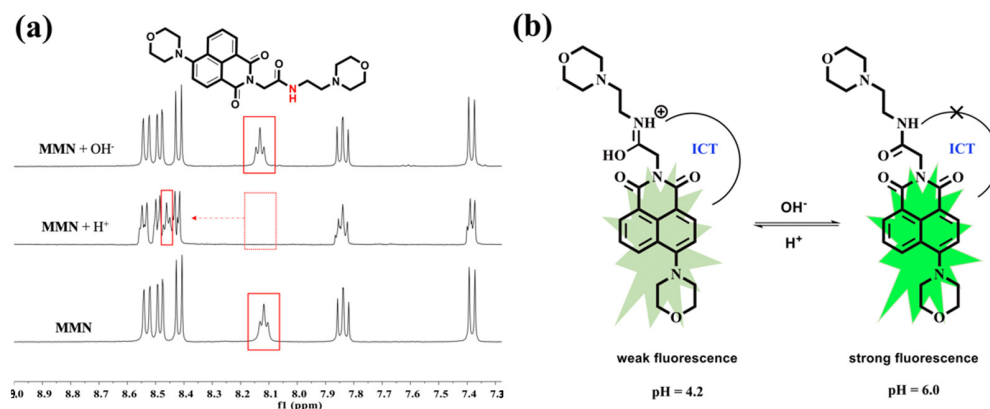

Figure 3. (**a**) The ^{1}H NMR spectra of probe **MMN**, **MMN + H$^+$** and **MMN + OH$^-$** in D$_2$O/DMSO-d_6 (*v*/*v*, 1:1). (**b**) Proposed sensing mechanism of **MMN** toward H$^+$.

2.5. Colocalization Imaging Experiment and Test Stri

The colocalization experiment was carried out using a commercial lysosome-specific dye, Lyso-Tracker Red, to confirm the lysosome-targeting ability of **MMN**. As shown in Figure 4, **MMN** displayed blue punctuated fluorescence (Figure 4b), which merged well with the red fluorescence produced by Lyso-Tracker Red (Figure 4d) and had a high Pearson's colocalization coefficient of 0.67 with an overlap coefficient of 0.99 (Figure 4e). Simultaneously, the intensity profile within the ROI in the blue and red channels displayed a trend of synchronization (Figure 4f). The results demonstrate that **MMN** could selectively locate lysosomes in live cells and has the potential to detect pH in lysosomal cells. This is evident in the test paper experiments shown in Figure 5. When the apparent pH decreased

from 6.0 to 4.2, the fluorescent colors of the test papers changed from light green to ivory by degrees. The dye strip results show that **MMN** can be used for rapid and portable pH monitoring. In addition, the performance of **MMN** was compared with other previously reported pH probes (Table 1) [28–30].
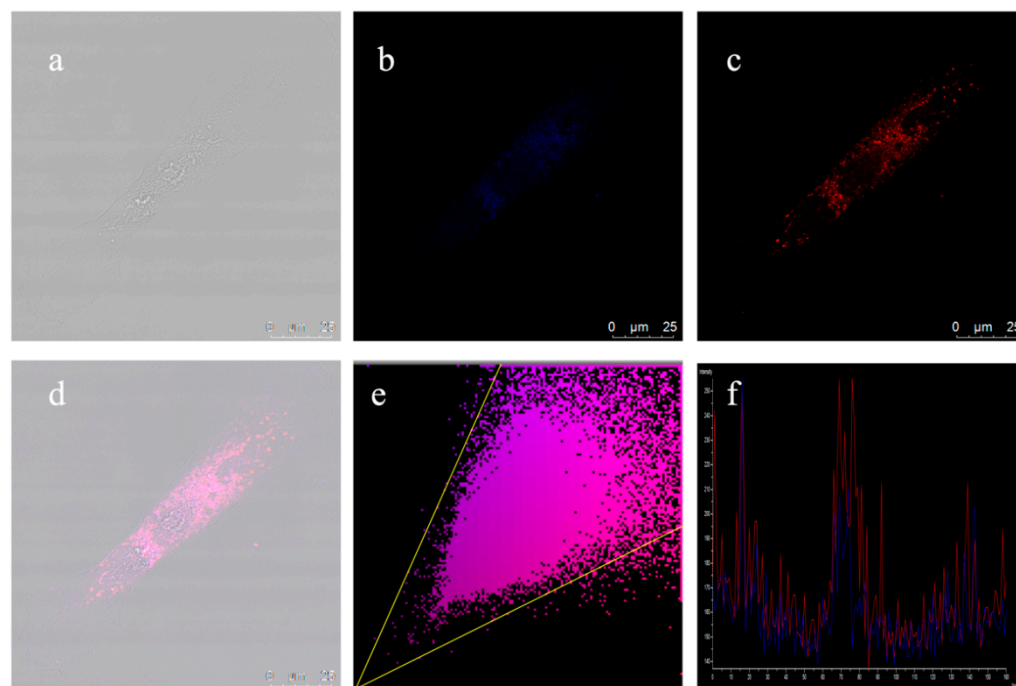
Figure 4. (**a**) Bright field images. (**b**) MMN(λ_{em} = 415 nm). (**c**) Lyso-Tracker Red (λ_{em} = 577 nm). (**d**) Merge images of (**a–c**). (**e**) The intensity scatter plot of blue channel and red channel. (**f**) Intensity profile of ROI across the cells in the red and blue channels.

Figure 5. The photographs of **MMN** on test papers with different apparent pH solutions under a UV lamp (365 nm).

Table 1. Comparison with other reported pH probes based on naphthalimide.

| Type	Working Media	Sensitive Range (pH)	Sensing Mechanism	Application	References
Off–on	MeCN/H_2O (9/1)	4.2–6.0	ICT	Paper strip/Targetable Imaging/pesticide detection	**MMN**
On–off	PBS buffer	5.0–7.2	PET	Cell imaging	[28]
Off–on–off	H_2O	2.0–10	PET	-	[29]
Colorimetric probe	DMSO	4.5–8.0	FRET	Cell imaging	[30]

2.6. Detection of Isoxaflutole

To further investigate the detection properties of **MMN, MMN** was placed in a CH_3CN solution along with different pesticides, including triketones, fluorine, cyanide and isoxazole. In the fluorescence spectra (Figure 6a), the addition of isoxaflutole to the solution of **MMN** induced obvious fluorescence quenching, while the other pesticides exerted a negligible influence under the same conditions. Similarly, the **MMN** solution could be clearly observed only when isoxaflutole was added and the fluorescence changed from strongly green to quenched (inset in Figure 6a). When isoxaflutole was added to the probe

solution, the absorption spectrum was not affected at 400 nm and a new strong absorption band appeared, centered at 293 nm. (Figure S3). The results indicate that **MMN** could be used to distinguish isoxaflutole from these other pesticides. To further illustrate the specific detection of isoxaflutole by **MMN**, the fluorescence spectra of **MMN** were investigated when other pesticides existed in the background. As shown in Figure 6b, no noticeable fluorescence interference from other pesticides was observed, revealing that **MMN** possesses high selectivity as a disturbance-free isoxaflutole fluorescent probe.
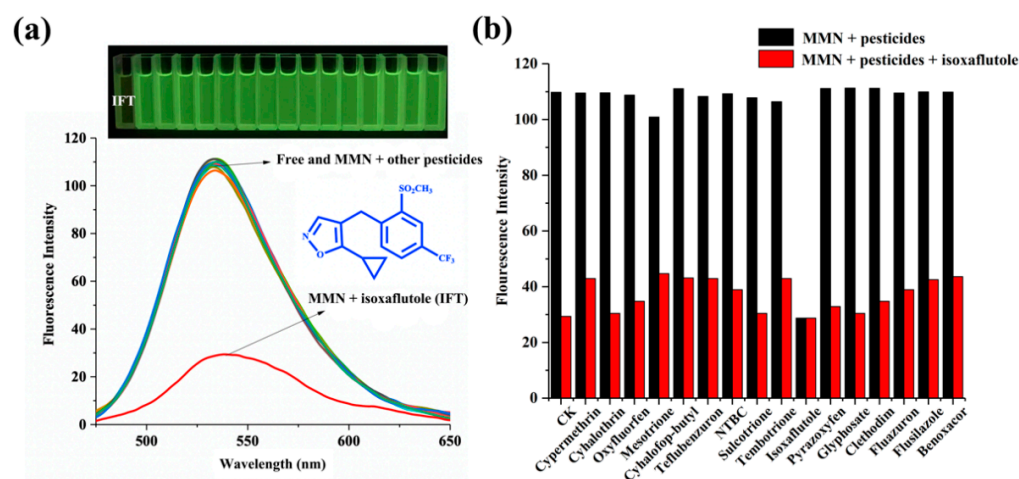

Figure 6. (**a**) Fluorescence spectra changes of the **MMN** solution (10 µM) after adding different pesticides (50 µM). Inset: color changes of **MMN** solution before and after adding pesticides under UV light of 365 nm. (**b**) Competition selectivity of **MMN** (10 µM) toward isoxaflutole (50 µM) in the presence of other competition pesticides (100 µM).

For a sensitivity analysis, a fluorescence titration study of **MMN** was conducted in the presence of various concentrations of isoxaflutole. The intensity of fluorescence at 529 nm decreased gradually with the addition of an increasing amount of isoxaflutole (Figure 7a). The emission intensity stabilized after the amount of added isoxaflutole ion reached 5 equiv. and showed a linear relationship (R^2 = 0.98 or 0.99) with the concentration of isoxaflutole in the ranges of 10–27 or 28–50 µM (inset in Figure 7a). Moreover, based on the equation LOD = $3\sigma/k$, the LOD of **MMN** for isoxaflutole was determined to be 0.88 µM, where σ is the standard deviation of the response at the lowest concentrations and k represents the slope of the calibration. The results indicate that **MMN** could be used to quantitatively determine isoxaflutole with a low detection limit. The binding constant of **MMN** with isoxaflutole was calculated according to the fluorescence intensity data using the modified Stern–Volmer equation: $I_0/(I_0 - I) = 1/A + 1/K \cdot 1/[Q]$ [31], where I_0 and I are the maximum luminescent intensities of **MMN** before and after adding isoxaflutole, K is the binding constant (M^{-1}) and the unit measurement [A] represents molar concentration. The binding constant (K) was calculated as $3.7 \times 10^5\ M^{-1}$ (Figure 7b), which was compared with other previously reported fluorescent probes (Table S1). Considering that response time is a crucial factor for photostability, the time-dependent curve was studied, as shown in Figure S4. The results demonstrate that the fluorescence signal of free **MMN** remained stable while **MMN** showed immediate and distinct fluorescence quenching; the fluorescence intensity reached the minimum within 30 s and remained stable in the following 90 min, indicating a high reactivity of **MMN** with isoxaflutole.
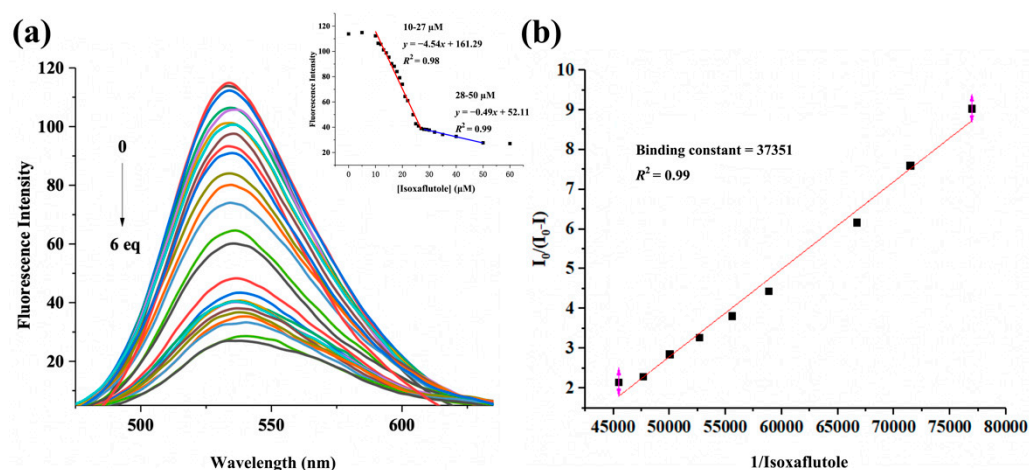
Figure 7. (**a**) Fluorescence spectra recorded for probe **MMN** (10 μM) upon spectrometric titration with isoxaflutole (0–60 μM). Inset: The relationship between the fluorescence intensity and the concentration of isoxaflutole. (**b**) Stern–Volmer plot of **MMN** between **MMN** and isoxaflutole.

A Job's plot analysis was carried out to determine the stoichiometric ratios of **MMN** to isoxaflutole,. The emission intensity reached the maximum when the molar fraction of isoxaflutole was 0.5, which indicates that **MMN** and isoxaflutole act in a stoichiometric ratio of 1:1 (Figure S5). The possible mechanism of **MMN** for detecting pesticides was investigated by density functional theory (DFT) calculations exhibited via the electron density or energy level between isoxaflutole and **MMN**. As shown in Figure 8, several representative pesticide molecules for DFT were selected as examples for investigation. It was found that the LUMO energy levels of isoxaflutole and mesotrione were lower than those of other pesticides (glyphosate, oxyfluorfen, pyrazoxyfen and cypermethrin), indicating that the electron affinities of isoxaflutole with the -CF$_3$ electron-withdrawing group and mesotrione with the -NO$_2$ electron-withdrawing group were relatively higher than those of other pesticides. Meanwhile, their LUMO energy levels were between the HOMO and LUMO energy levels of **MMN**, which could cause the transition of electrons from the LUMO orbital of **MMN** to the LUMO orbitals of isoxaflutole and mesotrione in the excited state [32–37]. The transition of electrons from the LUMO orbital of **MMN** in the excited state to the LUMO of isoxaflutole prevented the electrons from returning to the HOMO orbital of **MMN**, leading to the phenomenon of fluorescence quenching in the recognition of isoxaflutole. The electron-withdrawing group in isoxaflutole may play a vital role in quenching effects due to the photoinduced electron transfer from **MMN** to electron-deficient isoxaflutole. Therefore, DFT illuminates the possible mechanism of how **MMN** detects isoxaflutole.
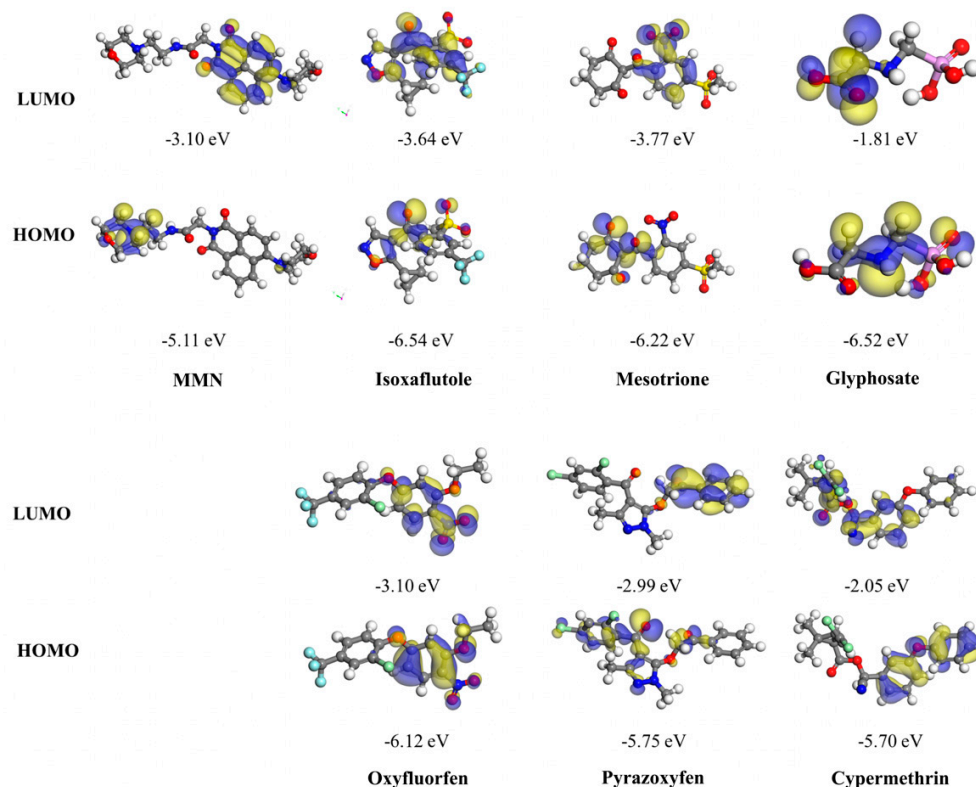
Figure 8. HOMO and LUMO molecular orbitals and relative energy levels of **MMN** and six pesticides.

3. Experimental Section

3.1. Materials and Methods

All reagents used in the experiment, including raw materials, solvents and pesticides, were purchased from commercial suppliers and used without purification. A Bruker ALPHA-T spectrometer (KBr, Bruker, Ettlingen, Germany) was used to record FTIR spectra. The ^{1}H NMR and ^{13}C NMR spectra of the samples were obtained using a Bruker AVANCE 400 MHz system (Bruker, Germany). High-resolution mass spectrometry (HRMS) was performed on an FTMS Ultra Apex MS spectrometer (Bruker Daltonics Inc., Billerica, MA, USA). UV–Vis and fluorescence spectra were measured on a UV-2550 ultraviolet spectrophotometer (Shimadzu, Kyoto, Japan) and a PerkinElmer LS55 fluorescence spectrometer (PerkinElmer, Buckinghamshire, UK), respectively. All pH values were measured with a PHS-3C pH meter (Inesa, Shanghai, China). Cell images were obtained on a LEICATCSSP2 confocal laser scanning microscope (Leica, Wetzlar, Germany).

3.2. Synthesis

3.2.1. Synthesis of 4-Morpholine-1,8-naphthalic Anhydride (**1**)

Compound **1** was synthesized based on the published literature [38]. 4-Bromo-1,8-naphthalic anhydride (5.54 g, 20.0 mmol) was added to 2-methoxyethanol (25 mL) in a three-necked flask and stirred at 25 °C until it dissolved. Then, 1.92 mL (22.0 mmol) of morpholine was dropped into the reaction system and the temperature was increased to 125 °C, after which the system was refluxed for 5 h. After cooling to room temperature, the insoluble orange needle-like precipitate was separated out. The residue was recrystallized from EtOH to obtain the final yellow needles (1). Yield: 90%. m.p.: 227.7–228.5 °C. All spectra of the structural characterization of compound **1** are presented in the electronic Supplementary Materials (Figures S6–S8). FT-IR (KBr) cm^{-1}: 3076, 2954, 2852 (v C-H), 1762, 1724 (v C=O). ^{1}H NMR (CDCl$_3$, TMS, 400 MHz, ppm) δ 8.61 (m, 1H), 8.55 (d, J = 8.1 Hz, 1H), 8.48 (m, 1H), 7.76 (m, 1H), 7.28 (s, 1H), 4.07–4.00 (m, 4H), 3.35–3.29 (m, 4H). ^{13}C NMR (CDCl$_3$, TMS, 100 MHz, ppm): 156.83, 134.88, 133.32, 131.57, 126.18, 115.26, 77.22, 66.83, 53.31.

3.2.2. Synthesis of *N*-Carboxymethyl-4-morpholine-1,8-naphthalimide (**2**)

Compound **2** was synthesized by improving the previous synthesis method [39]. A mixture of compound **1** (2.85 g, 10 mmol) and glycine (1.15 g, 15 mmol) was refluxed with continuous stirring in *N,N*-dimethylformamide (DMF) (75 mL) at 100 °C for 30 h. The filtrate was transferred to a water-filled beaker. After the yellow solid was completely separated out, the crude product was obtained by filtration, which was purified by recrystallization from ethanol to give compound **2**. Yield: 86%. m.p.: 247.7–248.4 °C. All spectra of the structural characterization of compound **2** are presented in the electronic Supplementary Materials (Figure S9–S11). FT-IR (KBr) cm^{-1}: 3435 (v OH), 2960, 2821 (v C-H), 1735, 1701,1658 (v C=O). ^{1}H NMR (DMSO-d_6, TMS, 400 MHz, ppm) δ 13.04 (s, 1H), 8.57–8.42 (m, 3H), 7.85 (m, 1H), 7.39 (d, *J* = 8.1 Hz, 1H), 4.72 (s, 2H), 3.97–3.84 (m, 4H), 3.29–3.19 (m, 4H). ^{13}C NMR (DMSO-d_6, TMS, 100 MHz, ppm): 169.88, 163.75, 163.16, 156.35, 133.05, 131.58, 131.51, 129.71, 126.70, 125.79, 122.57, 115.67, 66.64, 53.51, 41.50.

3.2.3. Synthesis of *N*-(2-Morpholinoethyl)acetamide-4-morpholine-1,8-naphthimide (**MMN**)

The compound *N*-(2-morpholinoethyl)acetamide-4-morpholine-1,8-naphthimide was prepared by adopting the reported procedure [40–42]. Compound **2** (5 mmol) was reacted with 4-(2-aminoethyl)morpholine by the coupling reagents 1-ethyl-3-(3-dimethylaminopropyl) carbodiimide (EDC, 1.1 eq), the base *N,N*-diisopropylethylamine (DIEA, 2 eq) and hydroxybenzotrizole (HOBt, 1.2 eq) in dry DMF. After 10 h, the reaction was quenched by adding water and the desired product was precipitated from the reaction mixture, which was filtered and dried. The mixture was purified by column chromatography on silica gel eluted with CH_2Cl_2/MeOH (v/v, 15/1). Yield: 75%. m.p. > 280 °C. All spectra of the structural characterization of compound **MMN** are presented in the electronic Supplementary Materials (Figure S12–S15). FT-IR (KBr) cm^{-1}: 3305 (v NH), 3097, 2924, 2854 (v C-H), 197, 1662 (v C=O). ^{1}H NMR (DMSO-d_6, TMS, 400 MHz, ppm) δ 8.54 (d, *J* = 8.5 Hz, 1H), 8.50 (d, *J* = 7.3 Hz, 1H), 8.43 (d, *J* = 8.1 Hz, 1H), 8.12 (s, 1H), 7.85 (s, 1H), 7.39 (m, 1H), 4.63 (s, 2H), 3.93 (t, *J* = 4.6 Hz, 4H), 3.56 (t, *J* = 4.7 Hz, 4H), 3.29–3.14 (m, 6H), 2.35 (m, 6H). ^{13}C NMR (DMSO-d_6, TMS, 100 MHz, ppm): 167.14, 163.92, 163.37, 156.08, 132.73, 131.21, 129.77, 126.61, 125.78, 123.03, 116.26, 115.56, 66.65, 55.38, 53.70, 53.52, 42.74; HRMS (ESI): calcd. for $C_{24}H_{28}N_4O_5$ ([M+H] $^+$) 453.2060, found 453.2144.

3.3. General Method for the Spectra Experiments of MMN

The stock solution of **MMN** was prepared in CH_3CN/H_2O (v/v, 9/1). The 1.00×10^{-2} M stock solutions of metal cations (KCl, NaCl, $AgNO_3$, $PbCl_2$, $SnCl_2$, $CoCl_2$, $CuCl_2$, $HgCl_2$, $BaCl_2$, $MnCl_2$, $CaCl_2$, $ZnCl_2$, $MgCl_2$, $NiCl_2$, $CrCl_3$, $FeCl_3$ and $AlCl_3$) were prepared with deionized water. The 1.00×10^{-2} M solutions of anions (F^-, Cl^-, Br^-, I^-, NO_3^-, NO_2^-, CN^-, SCN^- $H_2PO_4^-$, SO_4^{2-} and HSO_4^-) were prepared by tetrabutylammonium (TBA) salts and sodium salts with deionized water. The ionic salts were dissolved in distilled water to prepare the stock solutions for the cations and anions (1.00×10^{-2} M). The stock pesticide solutions (1.00×10^{-2} M) were prepared in DMSO due to the poor solubility of some pesticides using cypermethrin, cyhalothrin, oxyfluorfen, mesotrione, cyhalofop-butyl, teflubenzuron, NTBC, sulcotrione, tembotrion, isoxaflutole, pyrazoxyfen, glyphosate, clethodim, fluazuron, flusilazole, fluorobenzene and benoxacor. For different pH solutions, 1.00×10^{-1} M HCl or NaOH was added to 10 mL of 1.00×10^{-5} M **MMN** solution and the apparent pH value was determined with a pH meter. To investigate the anti-interference of **MMN**, 50 μL aliquots of 1.00×10^{-2} M different cation and anion solutions were used as the background to measure the fluorescence spectra at two representative apparent pH values (4.2 and 6.0). Different instruments were used for fluorescence spectroscopic detection of pH and isoxaflutole. The slit widths of excitation and emission were set to 10 nm, and the excitation wavelength was set to 415 nm in the fluorescence spectral experiment.

3.4. Cell Incubation and Fluorescence Imaging

Human stromal cell line (HSC) cells were purchased from the Chinese Academy of Sciences and cultured using the medium DMEM, which contains 15% fetal bovine serum, 100 μg/mL penicillin and 100 g/mL streptomycin at 37 °C within a humidified 5% CO_2 atmosphere. One day before the fluorescence imaging experiment, the cells were placed on petri dishes (NESTC) at the bottom of 35 mm cover slides. The cells were incubated with Lyso-Tracker Red (70 nM) for 30 min, washed with PBS 3 times, fixed with 4% paraformaldehyde for 1 h, washed with PBS 3 times, washed with a solvent 3 times, stained overnight with **MMN** (100 nM), washed with a solvent 3 times, sealed and observed under a confocal microscope.

3.5. Computational Methods

The Perdew–Burke–Ernzerh (PBE) method of Generalized Gradient Approximation (GGA) in the Dmol3 module was used to calculate the exchange correlation energy using a DNP+ basis set calculation and dispersion correction with Grimme [43–45].

4. Conclusions

In summary, we designed and developed a multifunctional naphthimide-based fluorescent probe (**MMN**). Because of the H^+-induced intramolecular charge transfer (ICT) effect, **MMN** displayed significant pH sensitivity with apparent pK_a values of 4.62 ± 0.02 and 5.43 ± 0.02 as well as good linear apparent pH responses ranging from 4.2 to 5.0 and from 5.0 to 6.0, which were suitable for selectively detecting acidic lysosomes. **MMN** shows potential for the rapid detection of pH in test papers. Furthermore, **MMN** could quickly and easily detect isoxaflutole with an extremely low detection limit. Density function theory calculations revealed MMN's potential underlying the sensing mechanism.

Supplementary Materials: The following are available online at https://www.mdpi.com/article/10.3390/ijms23116256/s1.

Author Contributions: F.Y. and Y.F. conceived and designed the experiment and conveyed the manuscript information as corresponding authors. L.Y. and Y.L. (Yan Liu) repeated the experiment multiple times and then applied the findings as in-depth research content. M.Y. used Origin and Excel to process the data. P.L. coordinated the data. Y.L. (Yulong Liu) consulted relevant literature, collected background knowledge and theoretical support. Y.L. (Yan Liu) synthesized and purified the compound. The manuscript was written by L.Y. and edited by F.Y. and Y.F. All authors have read and agreed to the published version of the manuscript.

Institutional Review Board Statement: Not applicable.

Informed Consent Statement: Not applicable.

Data Availability Statement: Not applicable.

Conflicts of Interest: The authors declare no conflict of interest.

References

1. Chao, J.B.; Wang, H.J.; Zhang, Y.B.; Li, Z.Q.; Liu, Y.H.; Huo, F.J.; Yin, C.X.; Shi, Y.W.; Wang, J.J. A single pH fluorescent probe for bio-sensing and imaging of extreme acidity and extreme alkalinity. *Anal. Chim. Acta* **2017**, *975*, 52–60. [CrossRef] [PubMed]
2. Grabe, M.; Oster, G. Regulation of organelle acidity. *J. Gen. Physiol.* **2001**, *117*, 329–344. [CrossRef] [PubMed]
3. Ambrosio, F.; Wiktor, J.; Pasquarello, A. pH-dependent catalytic reaction pathway for water splitting at the BiVO$_4$–water interface from the band alignment. *ACS Energy Lett.* **2018**, *3*, 829–834. [CrossRef]
4. Parks, S.K.; Chiche, J.; Pouysségur, J. pH control mechanisms of tumor survival and growth. *J. Cell. Physiol.* **2011**, *226*, 299–308. [CrossRef] [PubMed]

5.   Settembre, C.; Fraldi, A.; Medina, D.L.; Ballabio, A. Signals from the lysosome: A control centre for cellular clearance and energy metabolism. *Nat. Rev. Mol. Cell Biol.* **2013**, *14*, 283–296. [CrossRef] [PubMed]

6.   Xu, H.; Ren, D. Lysosomal physiology. *Annu. Rev. Physiol.* **2015**, *77*, 57–80. [CrossRef]

7.   Luka, G.S.; Nowak, E.; Kawchuk, J.; Hoorfar, M.; Najjaran, H. Portable device for the detection of colorimetric assays. *R. Soc. Open Sci.* **2017**, *4*, 171025. [CrossRef]

8.   Manjakkal, L.; Szwagierczak, D.; Dahiya, R. Metal oxides based electrochemical pH sensors: Current progress and future perspectives. *Prog. Mater. Sci.* **2020**, *109*, 100635. [CrossRef]

9.   Miao, Y.; Chen, J.; Fang, K. New technology for the detection of pH. *J. Biochem. Bioph. Meth.* **2005**, *63*, 1–9.

10. Ma, Q.; Zhuo, W.; Zhai, Z.; Gong, G.; Zhang, T.; Xiao, H.; Zhou, Z.; Liu, Y. A new fluorescent probe for neutral to alkaline pH and imaging application in live cells. *Spectrochim. Acta A* **2021**, *261*, 120031. [CrossRef]

11. Kang, T.; Gao, S.; Zhao, L.X.; Zhai, Y.; Ye, F.; Fu, Y. Design, synthesis and SAR of novel 1,3-disubstituted imidazolidine or hexahydropyrimidine derivatives as herbicide safeners. *J. Agric. Food Chem.* **2021**, *69*, 45–54. [CrossRef] [PubMed]

12. Pallett, K.E.; Cramp, S.M.; Little, J.P.; Veerasekaran, P.; Crudace, A.J.; Slater, A.E. Isoxaflutole: The background to its discovery and the basis of its herbicidal properties. *Pest Manage. Sci.* **2001**, *57*, 133–142. [CrossRef]

13. Stephenson, D.O.; Bond, J.A. Evaluation of thiencarbazone-methyl– and isoxaflutole-based herbicide programs in corn. *Weed Technol.* **2012**, *26*, 37–42. [CrossRef]

14. Simmons, J.T.; Kells, J.J. Variation and inheritance of isoxaflutole tolerance in corn (zea mays). *Weed Technol.* **2003**, *17*, 177–180. [CrossRef]

15. Nelson, E.A.; Penner, D. Leaching of isoxaflutole and the herbicide safeners R-29148 and furilazole. *Weed Technol.* **2007**, *21*, 106–109. [CrossRef]

16. Alletto, L.; Benoit, P.; Bergheaud, V.; Coquet, Y. Variability of retention process of isoxaflutole and its diketonitrile metabolite in soil under conventional and conservation tillage. *Pest Manag. Sci.* **2012**, *68*, 610–617. [CrossRef] [PubMed]

17. Rouchaud, J.; Nues, O.; Eelen, H.; Bulcke, R. Soil metabolism of isoxaflutole in corn. *Arch. Environ. Contam. Toxicol.* **2002**, *42*, 280–285. [CrossRef]

18. Lin, C.H.; Lerch, R.N.; Thuiman, E.M.; Garrett, H.E.; George, M.F. Determination of isoxaflutole (balance) and its metabolites in water using solid phase extraction followed by high-performance liquid chromatography with ultraviolet or mass spectrometry. *J. Agric. Food Chem.* **2002**, *50*, 5816–5824. [CrossRef] [PubMed]

19. Lin, C.H.; Lerch, R.N.; Garrett, H.E.; Li, Y.X.; George, M.F. Improved HPLC-MS/MS method for determination of isoxaflutole (balance) and its metabolites in soils and forage plants. *J. Agric. Food Chem.* **2007**, *55*, 3805–3815. [CrossRef] [PubMed]

20. Ye, Z.; Xiong, C.; Pan, J.; Su, D.; Zeng, L. Highly photostable, lysosometargeted BODIPYs with green to near-infrared emission for lysosome imaging in living cells. *Dyes Pigm.* **2018**, *155*, 30–35. [CrossRef]

21. Zhang, Y.; Chen, H.; Chen, D.; Wu, D.; Chen, Z.; Zhang, J.; Chen, X.; Liu, S.; Yin, J. A colorimetric and ratiometric fluorescent probe for mercury (II) in lysosome. *Sens. Actuators B Chem.* **2016**, *224*, 907–914. [CrossRef]

22. Ye, F.; Wu, N.; Li, P.; Liu, Y.L.; Li, S.J.; Fu, Y. A lysosome-targetable fluorescent probe for imaging trivalent cations Fe^{3+}, Al^{3+} and Cr^{3+} in living cells. *Spectrochim. Acta A* **2019**, *222*, 117242. [CrossRef]

23. Zhou, H.; Feng, R.; Liang, Q.; Su, X.; Deng, L.; Yang, L.; Ma, L.J. A sensitive pH fluorescent probe based on triethylenetetramine bearing double dansyl groups in aqueous solutions and its application in cells. *Spectrochim. Acta A* **2020**, *229*, 117881. [CrossRef]

24. Fu, Y.; Pang, X.X.; Wang, Z.Q.; Chai, Q.; Ye, F. A highly sensitive and selective fluorescent probe for determination of Cu (II) and application in live cell imaging. *Spectrochim. Acta A* **2019**, *208*, 198–205. [CrossRef]

25. Ye, F.; Liang, X.M.; Xu, K.X.; Pang, X.X.; Chai, Q.; Fu, Y. A novel dithiourea-appended naphthalimide "on-off" fluorescent probe for detecting Hg^{2+} and Ag^+ and its application in cell imaging. *Talanta* **2019**, *200*, 494–502. [CrossRef]

26. Dong, B.; Song, X.; Kong, X.; Wang, C.; Zhang, N.; Lin, W. A tumor-targeting and lysosome-specific two-photon fluorescent probe for imaging pH changes in living cells. *J. Mater. Chem. B* **2017**, *5*, 988–995. [CrossRef] [PubMed]

27. Liu, L.J.; Guo, P.; Chai, L.; Shi, Q.; Xu, B.H.; Yuan, J.P.; Wang, X.G.; Shi, X.F.; Zhang, W.Q. Fluorescent and colorimetric detection of pH by a rhodamine-based probe. *Sens. Actuators B Chem.* **2014**, *194*, 498–502. [CrossRef]

28. Dong, Y.; Xiao, H.; Xing, L.; Wu, C.; Zhou, J.; Zhou, Z.; Liu, Y.; Zhuo, S.; Li, P. Two-photon fluorescence visualization of lysosomal pH changes during mitophagy and cell apoptosis. *Talanta* **2020**, *209*, 120549. [CrossRef]

29. Georgiev, N.I.; Yaneva, I.S.; Surleva, A.R.; Asiri, A.M.; Bojinov, V.B. Synthesis, sensor activity and logic behavior of a highly water–soluble naphthalimide derivative. *Sens. Actuators B Chem.* **2013**, *184*, 54–63. [CrossRef]

30. Ding, Z.; Liu, G.; Hu, J. Ratiometric fluorescent mapping of pH and glutathione dictates intracellular transport pathways of micellar nanoparticles. *Biomacromolecules* **2020**, *21*, 3436–3446. [CrossRef]

31. Yang, L.; Liu, Y.L.; Liu, C.G.; Fu, Y.; Ye, F. A built-in self-calibrating luminescence sensor based on RhB@Zr-MOF for detection of cations, nitro explosives and pesticides. *RSC Adv.* **2020**, *10*, 19149–19156. [CrossRef] [PubMed]

32. Yang, L.; Liu, Y.L.; Liu, C.G.; Fu, Y.; Ye, F. A cationic metal-organic framework for dye adsorption and separation based on column-chromatography. *J. Mol. Liq.* **2020**, *300*, 112311. [CrossRef]

33. Yang, L.; Liu, Y.L.; Ji, X.X.; Liu, C.G.; Fu, Y.; Ye, F. A novel luminescent sensor based on Tb@UiO-66 for highly detecting Sm^{3+} and teflubenzuron. *J. Taiwan Inst. Chem. Eng.* **2021**, *126*, 173–181. [CrossRef]

34. Liu, Y.; Li, L.; Yue, M.; Yang, L.; Sun, F.; Xu, G.; Fu, Y.; Ye, F. A switch-on fluorescent probe for detection of mesotrione based on the straight forward cleavage of carbon-nitrogen double bond of Schiff base. *Chem. Eng. J.* **2022**, *430*, 132758. [CrossRef]

35. Yang, L.; Liu, Y.L.; Liu, C.G.; Ye, F.; Fu, Y. Two luminescent dye@MOFs systems as dual-emitting platforms for efficient pesticides detection. *J. Hazard. Mater.* **2020**, *381*, 120966. [CrossRef] [PubMed]

36. Sun, F.; Yang, L.; Li, S.; Wang, Y.; Wang, L.; Li, P.; Ye, F.; Fu, Y. New fluorescent probes for the sensitive determination of glyphosate in food and environmental samples. *J. Agric. Food Chem.* **2021**, *69*, 12661–12673. [CrossRef] [PubMed]

37. Li, L.; Gao, S.; Yang, L.; Liu, Y.L.; Li, P.; Ye, F.; Fu, Y. Cobalt (II) complex as a fluorescent sensing platform for the selective and sensitive detection of triketone HPPD inhibitors. *J. Hazard. Mater.* **2021**, *404*, 124015. [CrossRef]

38. Dai, H.; Xu, H. Selective and sensitive fluorescent chemosensors for Cu^{2+} ion based upon bis-1,8-naphthalimide dyads. *Chin. J. Chem.* **2012**, *30*, 267–272. [CrossRef]

39. Liang, S.; Yu, H.; Xiang, J.; Yang, W.; Chen, X.; Liu, Y.; Gao, C.; Yan, G. New naphthalimide modified polyethylenimine nanoparticles as fluorescent probe for DNA detection. *Spectrochim. Acta A* **2012**, *97*, 359–365. [CrossRef]

40. Johansen, M.D.; Kremer, L.; Kumar, V. Variedly connected 1,8-naphthalimide-7-chloroquinoline conjugates: Synthesis, anti-mycobacterial and cytotoxic evaluation. *Bioorg. Chem.* **2019**, *92*, 103241. [CrossRef]

41. Zhou, L.; Jin, Z.; Fan, X.; Yao, Y.; Chen, Z.; Zhang, W.; Qian, J. Synthesis of 1,8-naphthalimide-based fluorescent nano-probes and their application in pH detection. *Chin. Chem. Lett.* **2018**, *29*, 1500–1502. [CrossRef]

42. Fu, Y.; Zhang, J.; Wang, H.; Chen, J.L.; Zhao, P.; Chen, G.R.; He, X.P. Intracellular pH sensing and targeted imaging of lysosome by a galactosyl naphthalimide-piperazine probe. *Dyes Pigm.* **2016**, *133*, 372–379. [CrossRef]

43. Adamo, C.; Barone, V. Toward reliable density functional methods without adjustable parameters: The PBE0 model. *J. Chem. Phys.* **1999**, *110*, 6158–6170. [CrossRef]

44. Frisch, M.J.; Pople, J.; Binkley, J.S. Self-consistent molecular orbital methods 25. Supplementary functions for Gaussian basis sets. *J. Chem. Phys.* **1984**, *80*, 3265–3269. [CrossRef]

45. Marenich, A.V.; Cramer, C.J.; Truhlar, D.G. Universal solvation model based on solute electron density and on a continuum model of the solvent defined by the bulk dielectric constant and atomic surface tensions. *J. Chem. Phys.* **2009**, *113*, 6378–6396. [CrossRef] [PubMed]